Consistency checks for two-body finite-volume matrix elements: II. Perturbative systems

Raúl A. Briceño,[1,2,*] Maxwell T. Hansen,[3,†] and Andrew W. Jackura[1,2,‡]

[1] *Thomas Jefferson National Accelerator Facility, 12000 Jefferson Avenue, Newport News, VA 23606, USA*
[2] *Department of Physics, Old Dominion University, Norfolk, Virginia 23529, USA*
[3] *Theoretical Physics Department, CERN, 1211 Geneva 23, Switzerland*

(Dated: December 3, 2019)

There is a broad need to study form-factor of multihadron states, from understanding the nature of hadronic resonances and bound-states in terms of their constituent quarks and gluons to the manifestation of beyond the Standard Model physics at low energies. With this goal in mind, a framework was developed to determine two-hadron form-factors by relating finite-volume matrix elements, computed from lattice QCD, to infinite-volume $\mathbf{2}+\mathcal{J}\to\mathbf{2}$ electroweak transition amplitudes. Following earlier studies of the formalism, we continue to provide non-trivial consistency checks in order to gain confidence in the framework. We explore the non-relativistic limit of a two-hadron system probed by a scalar current, showing that near threshold the finite-volume matrix element can be expressed as a series in the inverse volume of the box. We provide two confirmations of the analytic expansion. First, we evaluate the exact result numerically and explore the asymptotically large-volume limit. Second, we perform an independent analytical determination of the matrix element using time-ordered perturbation theory. This is similar in spirit to existing calculations in the literature, but unlikely previous result we include all diagrams appearing at the desired order.

I. INTRODUCTION

Understanding the emergence of hadrons from the interactions of their constituent quarks and gluons within quantum chromodynamics (QCD) has remained a challenge. In recent years, significant progress has been made in determining the properties of the ground-state hadrons via numerical calculations using lattice QCD [1–3]. Most hadrons, however, manifest as resonances in multihadron scattering processes, and are rigorously defined as pole singularities of scattering amplitudes. Computing resonance spectra, e.g. masses and decay widths, thus necessitates analytically continuing scattering amplitudes in the complex energy-plane to the pole. In addition to spectral properties, structural information of resonance such as charge radii or parton distribution functions must also be interpreted at the pole of form-factors, which are extracted from electroweak transition amplitudes.

Determining scattering phenomena directly from lattice QCD calculations is complicated by the fact that they are necessarily performed in a finite Euclidean spacetime, where one cannot formally construct asymptotic states. Presently, the most systematic method to overcome this issue is to derive and apply non-perturbative mappings between finite-volume spectra and matrix elements, which are directly calculable via numerical lattice QCD, and infinite-volume scattering and transition amplitudes. This methodology was first introduced by Lüscher [4, 5], where the finite-volume spectra of two hadrons in a cubic volume of length L was related to the elastic $\mathbf{2}\to\mathbf{2}$ scattering amplitude. Within this framework, on-shell intermediate states yield power-law finite-volume corrections $\mathcal{O}(L^n)$, while off-shell quantities are exponentially suppressed, $\mathcal{O}(e^{-m_\pi L})$. For sufficiently large box sizes, exponential correction can be neglected, giving systematic control over all power-law enhancements. Extensions of these ideas were developed to include moving frames, coupled channels, and particles with spin [6–14]. Applications of Lüschers methodology has proved effective for determining two-hadron bound and resonance states from lattice QCD [15–33], including energies where multiple channels are kinematically open [34–42]. The success of the two-hadron sector has led to the ideas of Lüscher being extended to $\mathbf{3}\to\mathbf{3}$ scattering [43–52], with spectral computations of $3\pi^+$ system beginning now [53–56]. [1]

Extensions of these finite-volume mappings have been made to extract electroweak transition amplitudes from lattice QCD calculations. As first studied in Ref. [59] for $K\to\pi\pi$ decays, finite-volume matrix elements computed in lattice QCD are related to electroweak transition amplitudes. This method has been generalized for arbitrary $\mathbf{1}+\mathcal{J}\to\mathbf{2}$ amplitudes [7, 10, 59–63] and applied in lattice QCD studies, such as $K\to\pi\pi$ decay amplitudes [64–67], $\gamma^\star\to\pi\pi$ [68, 69] and $\pi\gamma^\star\to\pi\pi$ [70–72] transition amplitudes near the ρ resonance, as well as a building block for

* e-mail: rbriceno@jlab.org
† e-mail: maxwell.hansen@cern.ch
‡ e-mail: ajackura@odu.edu

[1] For recent reviews on this topic we point the reader to Refs. [57, 58].

long range matrix elements [73–75]. Most recently, the formalism for $\mathbf{2}+\mathcal{J}\to\mathbf{2}$ electroweak transition amplitudes has been developed [76, 77]. These derivations supersedes previous attempts done at a finite order of a specific effective field theory [11, 78]. Unlike the $\mathbf{1}+\mathcal{J}\to\mathbf{2}$ scenario, the formalism in Refs. [76, 77] is more complicated due to the presence of additional finite-volume effects from triangle diagram topologies.

As the $\mathbf{2}+\mathcal{J}\to\mathbf{2}$ finite-volume mapping is complicated, it is necessary to provide various non-trivial checks on the formalism, and calculate limiting cases in which more straightforward predictions may be extracted. In a previous study [79], we explored the bound-state limit of matrix elements and recovered the expected result that finite-volume corrections are exponentially suppressed in the binding momentum as $L\to\infty$. However, just as in the spectrum [80–82], leading order contributions for box sizes $m_\pi L\sim 4-6$ were shown to yield significant deviations to the all-orders result of Refs. [76, 77], serving as a warning that one must consider the all-orders framework to reduce finite-volume systematics. Furthermore, in Ref. [79] we proved that this formalism in conjunction with the Ward-Takahashi identify protects the electromagnetic charge of finite-volume states.

We continue our study of consistency checks by investigating the near threshold limit for the finite-volume two-hadron matrix element. Above the two-particle threshold, finite-volume effects take the form of power-law enhancements in $1/L$. Near threshold, finite-volume spectra can be written as an expansion in the inverse volume [4, 83–86], as well as for matrix elements [87]. In Ref. [87], the authors carried out the expansion for n-scalar-bosons in the ground state, finding that the leading correction occurs at $\mathcal{O}(L^{-2})$ due to the triangle topology.

In this work, we derive a large-volume expansion for the finite volume two-hadron matrix elements near threshold. We focus on two identical scalar bosons which scatter dominantly in S wave, and which couple to an external scalar current. We briefly derive the well-known result for the large-volume expansion of the ground-state energy using the all-orders Lüscher formalism in Sec. II A. In Sec. II B, we follow the same methods to construct a large-volume expansion for the matrix element at zero-momentum transfer, using the all-orders result of Refs. [76, 77]. We numerically check this expression against the all-orders formalism in Sec. II C, confirming that the framework is self-consistent against the analytic prediction. We compare our result with that of Ref. [87], and find significant disagreement with their result, namely that our leading correction occurs at $\mathcal{O}(L^{-3})$ and even the $\mathcal{O}(L^{-3})$ term disagrees. Although we have included relativistic corrections, the source of the discrepancy is not just due to relativistic effects. In order to clarify the origin of the discrepancy, we provide an independent derivation of the near threshold matrix element using time-ordered perturbation theory in Sec. III. We find that the time-ordered perturbation theory result agrees with ours derived in Sec. II B. Additionally, we show that if we neglect the wavefunction renormalization and diagrams where the external legs are coupled to the external current, we recover the result in Ref. [87]. Finally, we summarize our findings in Sec. IV.

II. THRESHOLD EXPANSION

A. Finite volume spectra

We consider a two-particle system in a cubic box of size L, where the particles have mass m and are identical with respect to an external scalar current density $\mathcal{J}$. For simplicity, we assume throughout this article that the system has zero total momentum $\mathbf{P}=\mathbf{0}$, i.e. the system is in its center-of-momentum frame (CMF). Finite volume spectra of two particles, denoted by E_n, are related to infinite volume $\mathbf{2}\to\mathbf{2}$ partial wave amplitudes via the Lüscher quantization condition [4]. Generally, the quantization condition is a determinant over angular momentum space which holds below the first inelastic threshold and up to exponentially suppressed corrections of the form e^{-mL}. Since we are interested in the near threshold limit, equivalently the large L limit, we can safely ignore these exponential corrections. We make a further simplification by neglecting all partial waves higher than S-wave, leaving a simple algebraic condition

$$\mathcal{M}^{-1}(E_n)=-F(E_n,L), \tag{1}$$

where $\mathcal{M}$ is the S wave scattering amplitude and F is a known finite volume function. For our purposes, the scattering amplitude is most conveniently expressed in terms of a phase shift δ,

$$\mathcal{M}(E)=\frac{8\pi E}{\xi}\frac{1}{q\cot\delta-iq} \tag{2}$$

where ξ is a symmetry factor which is $1/2$ for identical particles and 1 otherwise, and q is the relative momentum of the two particles in the CMF defined via $E\equiv 2\sqrt{m^2+q^2}$. The finite-volume function can take on many forms, all equivalent up to exponentially suppressed corrections, as seen in Refs. [6, 7, 9, 13, 76]. For the S-wave case considered,

we express the finite volume function as

$$F(E,L) = \xi\left[\frac{1}{L^3}\sum\!\!\!\!\!\!\int_{\mathbf{k}}\right]\frac{1}{2\omega_{\mathbf{k}}}\frac{1}{E(E-2\omega_{\mathbf{k}}+i\epsilon)}$$
$$\equiv i\frac{\xi q}{8\pi E} + F_{\text{pv}}(E,L) \tag{3}$$

where

$$\left[\frac{1}{L^3}\sum\!\!\!\!\!\!\int_{\mathbf{k}}\right] \equiv \frac{1}{L^3}\sum_{\mathbf{k}\in(2\pi/L)\mathbb{Z}^3} - \int\frac{\mathrm{d}^3\mathbf{k}}{(2\pi)^3},$$

and in the second line explicitly removes the imaginary part of F, defining F_{pv}, which is the finite volume function with principal value prescription for the integral. Removing the imaginary part is useful as it exactly cancels the imaginary part of the scattering amplitude Eq. (2), leaving Eq. (1) as the real equation $\rho\cot\delta|_{E=E_n} = -F_{\text{pv}}(E_n,L)$. Equation (1) holds for all finite volume energies E_n up to corrections associated with higher partial waves and up to the first inelastic threshold and ignores exponentially suppressed corrections of the form e^{-mL}.

We proceed to solve Eq. (1) for the lowest energy, the threshold energy $E_0(L)$, for a given a phase shift in the large L limit. In the infinite volume limit, $E_0(\infty) = 2m$, thus we will write the solution as a finite volume correction to the $L\to\infty$ limit,

$$\Delta E_0(L) \equiv E_0(L) - 2m = \frac{q_0^2}{m} - \frac{q_0^4}{4m^3} + \mathcal{O}\left(q_0^6\right), \tag{4}$$

where q_0 is the lowest Lüscher momentum associated with the Lüscher energy $E_0(L) \equiv 2\sqrt{m^2+q_0^2}$. The correction is further expressed as an expansion in $1/L$, which is equivalent to an expansion in q as $q\to 0$. Near threshold, the phase shift is most conveniently represented by an effective range expansion

$$q\cot\delta = -\frac{1}{a} + \frac{1}{2}rq^2 + \mathcal{O}(q^4), \tag{5}$$

which has a finite radius of convergence in the domain around $q=0$ set by the nearest singularity, e.g. the t-channel exchange branch cut. The expansion defines the scattering length and effective range, a and r, respectively. The finite volume function Eq. (3) has a pole as $q\to 0$ when $k=0$. We can explicitly remove this pole, and are left with a regular function of q for all $\mathbf{k}\neq\mathbf{0}$. Removing this pole, it is straightforward to show that the finite volume function has an expansion

$$F_{\text{pv}}(E;L) = \frac{\xi}{2Eq^2L^3}\left[1 - \sum_{j=1}^{\infty}\left(\frac{qL}{2\pi}\right)^{2j}\mathcal{I}_j\right] \tag{6}$$

where $\mathcal{I}_j$ are geometric constants characterizing the finite cubic volume,

$$\mathcal{I}_j = \begin{cases} \left[\displaystyle\sum_{\mathbf{n}\neq\mathbf{0}} - \int \mathrm{d}^3\mathbf{n}\right]\frac{1}{n^2} & j=1 \\ \displaystyle\sum_{\mathbf{n}\neq\mathbf{0}}\frac{1}{n^{2j}} & j\geq 2, \end{cases}$$

with $n=|\mathbf{n}|$ such that $\mathbf{n}\in\mathbb{Z}^3$ for the finite volume sums [2]. The first three terms are are the usual constants found in the literature, e.g. the first three terms are

$$\mathcal{I}_1 = \mathcal{I}, \quad \mathcal{I}_2 = \mathcal{J}, \quad \mathcal{I}_3 = \mathcal{K}, \tag{7}$$

[2] A convenient method to evaluate these geometric constants is given in Ref. [86], which uses an exponential damping function to regularize the divergent terms.

where the numerical values can be found in, e.g., Ref. [87]. We leave the factor of E in the denominator of Eq. (6) un-expanded as it cancels exactly with the normalization given in Eqs. (2).

Using the expansions Eqs. (5) and (6) in Eq. (1), one can perform a series reversion to obtain q_0 as a series in powers of $1/L$. Substituting this result into Eq. (4), we obtain the volume corrections to the threshold energy

$$\Delta E_0(L) = \frac{4\pi a}{mL^3} \sum_{j=0}^{\infty} \gamma_j \left(\frac{a}{\pi L}\right)^j . \tag{8}$$

The ratio $a/\pi L$ is a convenient dimensionless constant parameter to characterize the expansion. Up to $\mathcal{O}(L^{-6})$, the expansion coefficients are

$$\begin{aligned}
\gamma_0 &= \quad 1 \\
\gamma_1 &= -\mathcal{I} \\
\gamma_2 &= \quad \left(\mathcal{I}^2 - \mathcal{J}\right) \\
\gamma_3 &= -\left(\mathcal{I}^3 - 3\mathcal{I}\mathcal{J} + \mathcal{K}\right) + \frac{2\pi^4 r}{a} - \frac{\pi^4}{m^2 a^2}.
\end{aligned}$$

The last term in α_3, which arises from the first relativistic correction $\mathcal{O}(q^4)$ in Eq. (4), in agreement with the expansion obtained in Ref. [85].

B. Matrix elements

Turning our attention to matrix elements, we now derive an $L \to \infty$ expansion for the matrix element of a $\mathbf{2}+\mathcal{J} \to \mathbf{2}$ system where $\mathcal{J}$ is a scalar current density. We work with the same two-particle system considered in the previous section, with both the initial and final state momentum being zero. In the S wave limit, the formalism presented in Refs. [76, 77] greatly simplifies to a single scalar relation of the initial and final finite-volume energies E_n and E'_n, respectively, and the box size,

$$L^3 \langle E'_n, L | \mathcal{J} | E_n, L \rangle = \mathcal{W}_{L,\mathrm{df}}(E'_n, E_n, L) \sqrt{\mathcal{R}(E'_n, L)\mathcal{R}(E_n, L)}, \tag{9}$$

which is valid up to the first inelastic threshold and higher partial waves, and ignores corrections of the form e^{-mL}. Here, $\mathcal{R}$ is the Lellouch-Lüscher factor

$$\begin{aligned}
\mathcal{R}(E_n, L) &\equiv \lim_{E \to E_n} \frac{E - E_n}{F^{-1}(E, L) + \mathcal{M}(E)} \\
&= \lim_{E \to E_n} \frac{-\mathcal{M}^{-2}(E_n)}{\dfrac{\partial}{\partial E}\left(F_{\mathrm{pv}}(E, L) + \dfrac{\xi q}{8\pi E} \cot \delta\right)},
\end{aligned} \tag{10}$$

and $\mathcal{W}_{L,\mathrm{df}}$ is a finite volume quantity defined as

$$\mathcal{W}_{L,\mathrm{df}}(E', E, L) = \mathcal{W}_{\mathrm{df}}(E', E) + f(Q^2)\, \mathcal{M}(E')\, G(E', E, L)\, \mathcal{M}(E). \tag{11}$$

Here, $f(Q^2)$ is the on-shell single particle form-factor with momentum transfer $Q^2 \equiv -(E' - E)^2$, for which the scalar charge defined as $g \equiv f(0)$, and G is a finite volume function defined in this case as

$$G(E', E, L) = \left[\frac{1}{L^3} \sum\!\!\!\!\!\!\int_{\mathbf{k}}\right] \frac{1}{2\omega_{\mathbf{k}}} \frac{1}{E'(E' - 2\omega_{\mathbf{k}} + i\epsilon)} \frac{1}{E(E - 2\omega_{\mathbf{k}} + i\epsilon)}. \tag{12}$$

Finally, $\mathcal{W}_{\mathrm{df}}$ is the infinite volume divergence free $\mathbf{2} + \mathcal{J} \to \mathbf{2}$ amplitude. Divergence free here means that all amplitudes where the current probes one of the external legs, leading to long-range singularities, are removed (see Refs. [76, 77] for a more detailed discussion on its relation to infinite-volume matrix elements). The $\mathcal{W}_{\mathrm{df}}$ amplitude has two types of kinematic singularities: (i) normal threshold singularities arising from the two-particle initial and final state interactions, analogous to those in the usual $\mathbf{2} \to \mathbf{2}$ scattering amplitude, and (ii) anomalous triangle singularities, which occur when all intermediate states of the triangle topology shown in Fig. 1 first go on-shell. For convenience, we define a two-hadron form-factor $\mathcal{F}$ as

$$\mathcal{W}_{\mathrm{df}}(E', E) = \mathcal{M}(E')\, \mathcal{F}(E', E)\, \mathcal{M}(E), \tag{13}$$

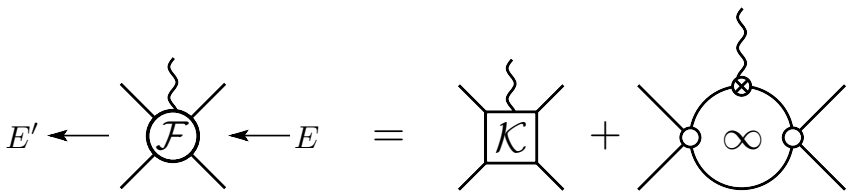

Figure 1. Diagrammatic representation of the two-hadron form-factor, $\mathcal{F}(E', E)$, given in Eq. (14). The first term is a real function containing short-range dynamics, and the second term is the triangle diagram contribution, which contains an imaginary part when the intermediate state particles go on-shell.

where $\mathcal{M}$ is given by Eq. (2) removes the initial and final state two-particle interactions. The two-hadron form-factor in turn, contains two contributing terms (see Fig. 1),

$$\mathcal{F}(E', E) = \mathcal{K}(E', E) + f(Q^2) G_\infty(E', E), \tag{14}$$

where $\mathcal{K}(E', E)$ is a real function in the elastic domain, similar to the $\mathbf{2} \to \mathbf{2}$ K matrix, which absorbs all short-range contributions from the amplitude and is to be determined from lattice QCD. The second function $G_\infty(E', E)$ is the triangle amplitude

$$G_\infty(E', E) = \int \frac{\mathrm{d}^3\mathbf{k}}{(2\pi)^3} \frac{1}{2\omega_\mathbf{k}} \frac{1}{E'(E' - 2\omega_\mathbf{k} + i\epsilon)} \frac{1}{E(E - 2\omega_\mathbf{k} + i\epsilon)}, \tag{15}$$

which allows for the possibility that the intermediate states go on-shell, thus providing an imaginary component. Equation (15) contains the same singularities as Eq. (12).

For the remainder of this article, we focus on the special case where $E' = E$, i.e. evaluating the matrix element at zero momentum transfer. If the current does not inject momentum, the G function simplifies, and we can remove the imaginary part as

$$\begin{aligned} G(E, E, L) &= \left[\frac{1}{L^3} \sum\!\!\!\!\!\!\int_\mathbf{k} \right] \frac{1}{2\omega_\mathbf{k}} \frac{1}{E^2(E - 2\omega_\mathbf{k} + i\epsilon)^2}, \\ &\equiv -i \frac{1}{32\pi E q} + G_\mathrm{pv}(E, E, L), \end{aligned} \tag{16}$$

where G_pv is the principal part of the G function. The infinite-volume triangle amplitude Eq. (15) has the same decomposition as Eq. (16), with the imaginary part having opposite side. See Appendix A for a derivation of the imaginary part of the triangle amplitude. Isolating the imaginary part from G_∞ allows us to absorb all other real parts into a single real function, defined as $\mathcal{F}_\mathrm{pv} \equiv \mathcal{K} + G_{\infty,\mathrm{pv}}$, so that the two-hadron form-factor reads

$$\mathcal{F}(E, E) \equiv \mathcal{F}_\mathrm{pv}(E, E) + i \frac{g}{32\pi E q}. \tag{17}$$

Substituting the finite- and infinite-volume functions at zero momentum transfer into Eq. (9), and simplifying gives our all-orders S wave matrix element

$$L^3 \langle E_n, L | \mathcal{J} | E_n, L \rangle = \frac{\mathcal{F}_\mathrm{pv}(E_n, E_n) + g\, G_\mathrm{pv}(E_n, E_n, L)}{-\frac{\partial}{\partial E}\left(F_\mathrm{pv}(E, L) + \frac{\xi}{8\pi E} q \cot\delta \right)\Big|_{E=E_n}}. \tag{18}$$

Given the spectrum obtained from Eq. (1) and matrix elements computed from lattice QCD, Eq. (18) can be used to solve for the unknown $\mathcal{F}_\mathrm{pv}$.

Having defined $\langle E_0, L | \mathcal{J} | E_0, L \rangle$ in terms of regular functions, we can now turn our attention to the large L expansion. As before, we expand each quantity in a series $q \to 0$, and substitute Eq. (8). First, since $\mathcal{F}_\mathrm{pv}$ is a regular function as $q \to 0$, it admits a series expansion similar to Eq. (5)

$$\mathcal{F}_\mathrm{pv}(E, E) = \mathcal{F}_0 + \mathcal{O}(q^2), \tag{19}$$

with $\mathcal{F}_0$ being a constant. Up to $\mathcal{O}(L^{-4})$ corrections, it is unnecessary to include higher terms in $\mathcal{F}_\mathrm{pv}$.

Next, the finite volume G function follows a similar expansion as Eq. (6), with now a pole as q^4. Using Eq. (A4) in the appendix, we can easily evaluate this function as in terms of a derivative on $F_{\rm pv}$,

$$\begin{aligned} G_{\rm pv}(E,E,L) &= -\frac{1}{4E}\frac{\partial}{\partial q^2}\left[\frac{2E}{\xi}F_{\rm pv}(E,L)\right], \\ &= \frac{1}{4Eq^4L^3}\left[1+\sum_{j=1}^{\infty}(j-1)\left(\frac{qL}{2\pi}\right)^{2j}\mathcal{I}_j\right]. \end{aligned} \tag{20}$$

Rewriting the the denominator of Eq. (18) as a derivative with respect to q^2, expanding each function in powers of q^2, and subsequently expanding q^2 in powers of L using Eq. (8), we find

$$\begin{aligned} L^3\langle E_0,L|\,\mathcal{J}\,|E_0,L\rangle &= \frac{\mathcal{F}_0+\mathcal{O}(q^2)+\dfrac{g}{4Eq^4L^3}\left[1+\sum_{j=1}^{\infty}(j-1)\left(\dfrac{qL}{2\pi}\right)^{2j}\mathcal{I}_j\right]}{-\dfrac{\xi}{16\pi}\dfrac{\partial}{\partial q^2}\left(\dfrac{4}{q^2L^3}\left[1-\sum_{j=1}^{\infty}\left(\dfrac{qL}{2\pi}\right)^{2j}\mathcal{I}_j\right]+q\cot\delta\right)\Big|_{E=E_n}}, \\ &= \frac{g}{2m\xi}\sum_{j=0}^{\infty}\beta_j\left(\frac{a}{\pi L}\right)^j, \end{aligned} \tag{21}$$

where the coefficients up to $\mathcal{O}(L^{-4})$ are given by

$$\begin{aligned} \beta_0 &= 1 \\ \beta_1 &= 0 \\ \beta_2 &= 0 \\ \beta_3 &= -\frac{2\pi^4}{m^2a^2}+\frac{2\pi^4}{a}\left(r+\frac{64\pi m}{g}\mathcal{F}_0\right) \\ \beta_4 &= \left(\frac{2\pi^4}{m^2a^2}-\frac{4\pi^4}{a}\left(r+\frac{64\pi m}{g}\mathcal{F}_0\right)\right)\mathcal{I}. \end{aligned} \tag{22}$$

The leading order term represents the pure single-hadron contribution which arises from the G-function, while the two-hadron form-factor $\mathcal{F}_0$ is sub-leading along with relativistic corrections from the single-hadron term. Notably absent are terms proportional to $1/L$ and $1/L^2$.

C. Numerical confirmation

To verify our analytic expression for the threshold expansion, Eq. (21), we define a function

$$M_{\mathcal{J}} \equiv 2m\xi g^{-1}L^3\langle E_0,L|\,\mathcal{J}\,|E_0,L\rangle - \beta_0, \tag{23}$$

which is a normalized matrix element with the leading order (LO) term removed, and plot $M_{\mathcal{J}}(mL)^2$ and $M_{\mathcal{J}}(mL)^3$ as a function of mL for large values of mL (see Fig. 2). We evaluate the matrix element using the all-orders result Eq. (18), with fixed $ma = 0.1$ and $g/2m\xi = 1$, and vary the parameters mr and $m\mathcal{F}_0$. In the first column, $mr = 0$ and $m\mathcal{F}_0 = 0$, in the second $mr = 0.25$ and $m\mathcal{F}_0 = 0$, and in the third $mr = 0.25$ and $m\mathcal{F}_0 = 0.5$. The first row of Fig. 2 corresponds to $M_{\mathcal{J}}L^2$, and shows that as $mL \to \infty$, the all-orders matrix element asymptotes to zero, clear agreeing with the term in the expansion $\beta_2(ma/\pi)^2 = 0$. This feature is identical in each of the three cases examined. The second row, $M_{\mathcal{J}}(mL)^3$, shows the all-orders result asymptoting to a non-zero value, which corresponds to $\beta_3(ma/\pi)^3$ in the expansion. For the numerical values considered, $\beta_3(ma/\pi)^3 \approx -0.63, -0.62, 5.7$ for the first, second, and third case, respectively. The numerical results show that there is no contribution at $\mathcal{O}(L^{-2})$ and the first non-trivial correction occurs at $\mathcal{O}(L^{-3})$, in agreement with the analytic expression for the threshold expansion. We have checked that the large L numerical result for the $\mathcal{O}(L^{-4})$ coincides with our expansion.

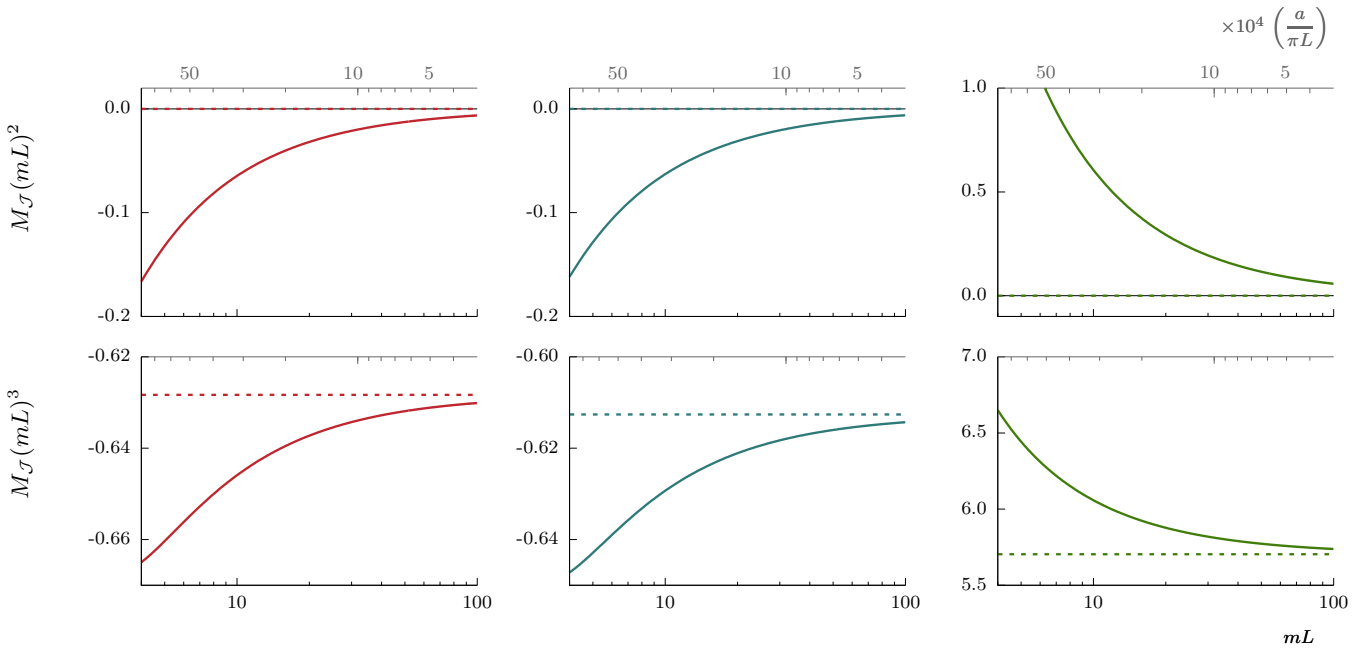

(a) $mr = 0$, $m\mathcal{F}_0 = 0$ (b) $mr = 0.25$, $m\mathcal{F}_0 = 0$ (c) $mr = 0.25$, $m\mathcal{F}_0 = 0.5$

Figure 2. Plots of $M_{\mathcal{J}}(mL)^2$ (top) and $M_{\mathcal{J}}(mL)^3$ (bottom) as a function of mL and $a/\pi L$, where $M_{\mathcal{J}}$ is defined in Eq. (23). The solid line is the exact matrix element computed from the all-orders result Eq. (18), and the dashed line corresponds to the asymptotic values $\beta_2(ma/\pi)^2$ (top) and $\beta_3(ma/\pi)^3$ (bottom) given by Eq. (22). All plots evaluated at fixed $g/2m\xi = 1$ and $ma = 0.1$. The first column (a) corresponds to scattering parameters $mr = 0$, and $m\mathcal{F}_0 = 0$, the second column (b) to $mr = 0.25$, $m\mathcal{F}_0 = 0$, and the third column (c) to $mr = 0.25$, $m\mathcal{F}_0 = 0.5$. For the given parameters, all three cases asymptote to $\beta_2(ma/\pi)^2 = 0$, in agreement with the threshold expansion in Eq. (21). The asymptotic values for the bottom row asymptote to $\beta_3(ma/\pi)^3 \approx -0.63$ for (a), -0.61 for (b), and 5.7 for (c) for their respective parameters.

D. Comparison with Ref. [87]

We compare the expansion given in Eq. (21) to that derived in Ref. [87]. To ease the comparison, we only consider terms up to to $\mathcal{O}(L^{-3})$. We begin by writing the expansion Eq. (21) explicitly to this order,

$$L^3 \langle E_0, L| \mathcal{J} |E_0, L\rangle = \frac{g}{2m\xi} - \frac{g}{2m\xi}\frac{2\pi a}{m^2 L^3} + \frac{g}{2m\xi}\frac{2\pi r a^2}{L^3} + \frac{(8\pi a)^2}{\xi}\frac{\mathcal{F}_0}{L^3} + \mathcal{O}(L^{-4}) \tag{24}$$

Identifying the leading order contributions from the single hadron and two hadron form-factor, we can relate to the coefficients in Ref [87]

$$\begin{aligned} 2\alpha_1(\text{Ref. [87]}) &\longleftrightarrow \frac{g}{2m\xi} \\ \alpha_2(\text{Ref. [87]}) &\longleftrightarrow \frac{(8\pi a)^2}{\xi}\mathcal{F}_0. \end{aligned} \tag{25}$$

The difference in the definitions of couplings can be identified to originate from (i) normalization of single-particle states and (ii) inclusion of initial/ final state interactions in the two-hadron transition amplitude (cf. Eq. (13)).

We reexpress Eq. (24) using the identifications in Eq. (25), giving

$$L^3 \langle E_0, L| \mathcal{J} |E_0, L\rangle = 2\alpha_1 - \frac{4\pi\alpha_1 a}{m^2 L^3} + \frac{4\pi\alpha_1 r a^2}{L^3} + \frac{\alpha_2}{L^3} + \mathcal{O}(L^{-4}). \tag{26}$$

At this point, we can compare with the main result of Ref. [87], which we only report to $\mathcal{O}(L^{-3})$,

$$L^3 \langle E_0, L| \mathcal{J} |E_0, L\rangle (\text{Ref. [87]}) = 2\alpha_1 + \frac{2\alpha_1 a^2}{\pi^2 L^2}\mathcal{J} + \frac{\alpha_2}{L^3} + \frac{4\alpha_1 a^3}{\pi^3 L^3}(\mathcal{K} - \mathcal{I}\mathcal{J}) + \mathcal{O}(L^{-4}). \tag{27}$$

First, we observe that the volume independent terms and the term containing α_2 (the two-hadron form-factor), are identical in both expansions at this order. It is easy to check that the α_2 term also agrees at $\mathcal{O}(L^{-4})$ as well.

For terms involving α_1, we find numerous discrepancies beginning at the first non-trivial correction, $\mathcal{O}(L^{-2})$. We see that such term is absent in our expansion, while seemingly present in the result of Ref. [87].

Our expansion contains terms at $\mathcal{O}(L^{-3})$ and $\mathcal{O}(L^{-4})$ proportional to α_1 and inversely proportional to m^2, whereas the expansion given in Ref. [87] do not contain m dependencies at these orders. These can be understood as relativistic corrections. These are of course absent in a non-relativistic determination of these matrix elements, which is arguably reasonable for determining nucleons but would be a poor approximation in general.

At $\mathcal{O}(L^{-3})$ we see corrections from the effective range, which are absent in Ref. [87]. This tension can removed by exploiting a present ambiguity of the relationship between $\mathcal{F}_0$ and α_2,

$$\alpha_2(\text{Ref. [87]}) \longleftrightarrow \frac{g}{2m\xi}\, 2\pi a^2 \left(r + \frac{64\pi m}{g}\mathcal{F}_0 \right). \tag{28}$$

This ambiguity lies in the fact that although α_2 is defined in Ref. [87] at the level of the Langrangian, a definition in terms of physical amplitudes is presently absent.

Furthermore, we have no terms of the form $\mathcal{O}((a/L)^3)$. This discrepancies unfortunately cannot be attributed to ambiguities in our identifications of α_1 or α_2 in Eq. (25). We can unambiguously identify $\alpha_1 = g/2m\xi$ by taking the infinite-volume limit of each respective matrix element. If we absorb remaining ambiguities into the definition of α_2, then although the $\mathcal{O}(L^{-3})$ terms will match, higher order terms will shift by the same amount, causing the discrepancy to persist.

It is worth reemphasizing that the tension with the results of Ref. [87] lie at the first non-trivial order, $\mathcal{O}(L^{-2})$, where the coefficient is fixed by the scattering length and the single-particle form factors. In other words, the tension is unambiguous.

The remainder of this article aims to verify our expansion and provide an explanation for the origin of this difference. In the next section we perform a perturbative expansion of the matrix element, and show the origin of the discrepancy with Ref. [87]. This is similar in spirit to what was done in Ref. [87], but we instead use a relativistic effective field theory.

III. PERTURBATIVE EXPANSION OF MATRIX ELEMENT

In this section, we provide an alternative derivation of the matrix element near threshold using time-ordered perturbation theory. We schematically follow the same approach as in Ref. [85], and refer the reader there for further details. The ingredients required are the two- and three-point finite volume correlation functions, which are subsequently written as a perturbation series in the interaction of the hadronic system, while keeping the current coupling at leading order. We work with a generalized effective field theory (EFT) of a scalar field with mass m, which is confined in a cubic box of length L, and coupled to an external scalar current.

Since we are interested in the scattering system near threshold, we work with the finite-volume correlator which creates and annihilates the two-particle state with zero relative momentum in its rest frame.

$$C_{2\text{pt}}(t) = \frac{(2m)^2\xi}{L^6} e^{2imt} \left\langle \tilde{\varphi}^2_{\mathbf{0}}(t) \tilde{\varphi}^{\dagger\,2}_{\mathbf{0}}(0) \right\rangle, \tag{29}$$

where $\tilde{\varphi}_{\mathbf{p}}(t)$ is an interpolating operator for a single scalar particle of momentum $\mathbf{p}$ at time t, which is related to the position-space and momentum space field operators via their respective Fourier transforms,

$$\tilde{\varphi}_{\mathbf{p}}(t) = \int_L \mathrm{d}^3\mathbf{x}\, e^{-i\mathbf{p}\cdot\mathbf{x}}\, \varphi(t,\mathbf{x}) = \int \frac{\mathrm{d}p_0}{2\pi} e^{-ip_0 t}\, \tilde{\varphi}(p). \tag{30}$$

The subscript L indicates that the spatial volume is restricted to a cube of side L, with periodic boundary conditions so that $\mathbf{p} = 2\pi\mathbf{n}/L$ with $\mathbf{n} \in \mathbb{Z}$. We assume the source and sink are time-ordered such that $t > 0$ always. The normalization of Eq. (29) is chosen such that the correlator is unity for non-interacting limit, coinciding with the conventions chosen in Ref. [85].

The two-point correlator can be written using the usual spectral representation,

$$C_{2\text{pt}}(t) = \sum_n Z_n e^{-iE_n t}, \tag{31}$$

where $\Delta E_n = E_n - 2m$. Since we focus solely on the threshold state, we will compute explicitly this correlator and ignore contributions from excited states. As discussed in Ref. [85], one can do this systematically since excited

state corrections will contribute at different powers of $1/L$ from the threshold state. Therefore, we can isolate all contributions to the threshold and ignore excited state terms. Defining the threshold correlator

$$C_{\text{2pt,th}}(t) = Z_0 e^{-i\Delta E_0 t}, \tag{32}$$

we can identify the wavefunction renormalization Z_0 and energy shift ΔE_0 in terms of $C_{\text{2pt,th}}$. As we shall see, we are only interested in the overlap, for which we have the simple relation

$$Z_0 = C_{\text{2pt,th}}(0). \tag{33}$$

In a similar manner, we define the 3-point correlation function which sums all-orders in the strong interaction, and is leading order in the external current, as

$$C_{\text{3pt}}(t', t) = \frac{(2m)^2 \xi}{L^6} e^{2im(t'-t)} \left\langle \tilde{\varphi}^2_{\mathbf{0}}(t') \mathcal{J}_1(0) \tilde{\varphi}^{\dagger\,2}_{\mathbf{0}}(t) \right\rangle, \tag{34}$$

where $\mathcal{J}_1$ is the single-hadron scalar current,

$$\mathcal{J}_1(x) = g\, \varphi(x) \varphi^\dagger(x), \tag{35}$$

where g is the scalar charge as before. Implicitly, we assume $t' > 0 > t$ to account for the time ordering. The normalization of Eq. (34) is chosen to coincide with the 2-point correlator. Since the discrepancy occurs in terms involving single-hadron coupling, we will not consider any current which couples to two hadrons. Nonetheless, the single-hadron current induces two-hadron effects which originate both from off-shell quantities and from the triangle topology, which we shall address in the derivation of the three-point correlator in Sec. III B. Following the procedure for the 2-point correlator, we isolate the threshold term from the spectral decomposition, giving

$$C_{\text{3pt,th}}(t', t) = Z_0 e^{-i\Delta E_0 (t'-t)} \left\langle E_0, L \right| \mathcal{J}_1 \left| E_0, L \right\rangle. \tag{36}$$

As for the 2-point correlator, we can always unambiguously separate exponentials contributing to excited states from the threshold states. The matrix element is time-independent, so we choose to compute the perturbation expansion of $C_{\text{3pt,th}}$ at $t' = t = 0$,

$$\left\langle E_0, L \right| \mathcal{J} \left| E_0, L \right\rangle = \frac{1}{Z_0} C_{\text{3pt,th}}(0, 0). \tag{37}$$

In the following subsections, we calculate $Z_0 = C_{\text{2pt,th}}(0)$ and $C_{\text{3pt,th}}(0, 0)$ order-by-order in time-ordered perturbation theory. To capture finite-volume corrections at $\mathcal{O}(L^{-3})$, we find we have to work to next-to-next-to-next-to-leading order (N3LO) in the strong interaction, as described in the following subsections.

Before proceeding to carry out the calculation, it is worth remarking how this differs in spirit with what was done in Refs. [76, 77] and consequently can provide an independent check. In [76, 77], the two-point and three-point correlation functions in momentum space were summed to all orders in terms of infinite-volume amplitude and finite-volume geometric functions. This followed from generalizations of the techniques presented in Ref. [7]. Having the all-orders result, one can then proceed to Fourier transform these correlators and match to their spectral decomposition to have relationships between finite-volume quantities (spectrum and matrix elements) and infinite-volume observables. Here, we instead consider the each individual diagram contribution to a given order in perturbation theory. By changing the orders of operations, this leads to important technical differences. For example, although in the all-order approach all diagrams where considered in this derivation, not all diagrams result in power-law finite-volume effects even though at a fixed order they might. In the derivation below we consider an important example of such diagrams, where the current couples to a final single-particle [see Figs. 4(b1-c2)]. These diagrams appear at the order being considered, and as a result are necessary to recover Eq. (21).

In order to facilitate this subsequent analysis we will make two simplifications. The first was previously mention, where we assume the current only couples to individual hadrons. The send is that we assume the scattering amplitude can be solely described a scattering lengths. In other words, we se the effective range and all other higher terms exactly to zero. These approximations are sufficient to illuminate the source of the tension without having to deal with further subtleties of perturbation theory.

A. Two-point correlator

We first examine the perturbative expansion of the two-point correlator. Instead of expressing the perturbation series around some strong coupling of our general EFT, we choose to organize it in terms of the Bethe-Salpeter kernel

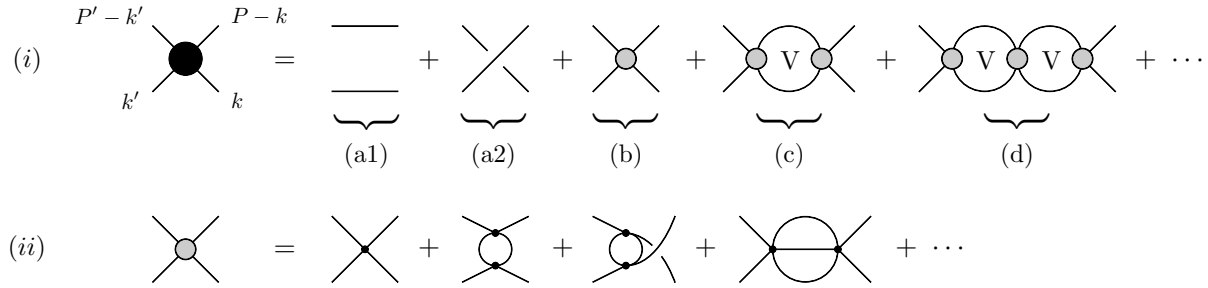

Figure 3. (i) Expansion of momentum space finite-volume two-point correlator in terms of the Bethe-Salpeter kernels. The normalization of the 2-point correlator, Eq. (29), is such that for the leading order contribution from the free propagators, diagrams (a1) and (a2), the correlator is unity. (ii) Low-order contributions to the Bethe-Salpeter kernel. Near threshold, only the S-wave terms are dominant.

$\mathcal{B}$, which contains all two-particle irreducible direct channel diagrams. We choose this for the following reasons: (i) in the kinematic domain of interest, these kernels are smooth functions, thus we may use the infinite-volume $\mathcal{B}$ since we ignore any exponentially suppressed correction. (ii), In the threshold limit, the momentum transfer between the initial and final state vanishes, leaving only the S wave amplitudes dominant. Moreover, the S wave Bethe-Salpeter kernels in this limit serve to renormalize the strong coupling. Therefore, we find that the Bethe-Salpeter kernel does not contribute to the threshold structures sought after in Eqs. (33) [85]. (iii) Expanding in $\mathcal{B}$ allows us to work with the free propagator since we can ignore self-energy corrections as they only contribute to exited state corrections in the correlator [85],

$$\langle \tilde{\varphi}_{\mathbf{0}}(t)\tilde{\varphi}^{\dagger}_{\mathbf{0}}(0)\rangle = L^3 \int \frac{\mathrm{d}k_0}{2\pi} e^{-ik_0 t} \frac{i}{k_0^2 - m^2 + i\epsilon} = L^3 \frac{e^{-imt}}{2m}, \tag{38}$$

where we closed the contour in the lower-half k_0-plane. (iv) Working with Bethe-Salpeter kernels allows us to easily identify order-by-order contributions from the infinite volume scattering amplitude via the Bethe-Salpeter equation. Ultimately, since we are interested in the threshold limit, we may write

$$\lim_{E=2m} \mathcal{M} = \lim_{E\to 2m} \sum_{n=1}^{\infty} \lambda^n \mathcal{M}^{(n)} = \lim_{E\to 2m} \left[-\frac{8\pi E}{\xi} \frac{a}{1 + iaq + \mathcal{O}(q^2)} \right] = -\frac{16\pi m a}{\xi}, \tag{39}$$

where λ is an expansion parameter which numerates the number of insertions of the Bethe-Salpeter kernel, such that $\lambda \to 1$ after calculation, and $\mathcal{M}^{(1)} = \mathcal{B}$.

Having our expansion procedure set, we expand the finite-volume correlators in the same manner, giving the expansion for the wavefunction renormalization,

$$Z_0 = 1 + \sum_{n=1}^{\infty} \lambda^n \, C^{(n)}_{\mathrm{2pt,th}}(0). \tag{40}$$

We have used the fact that the normalization in Eq. (29) fixes the leading order threshold correlator to unity. Our task now is to compute $C_{\mathrm{2pt,th}}(0)$ to $\mathcal{O}(\lambda^3)$, so that we may see all contributions up to $\mathcal{O}(L^{-3})$. In practice, it is convenient to write Eq. (29) in terms of its Fourier transform,

$$C_{\mathrm{2pt}}(t) = \frac{(2m)^2\xi}{L^6} e^{2imt} \int \frac{\mathrm{d}E'}{2\pi} \int \frac{\mathrm{d}E}{2\pi} \int \frac{\mathrm{d}k_0'}{2\pi} \int \frac{\mathrm{d}k_0}{2\pi} \, e^{-iE't} \, \langle \tilde{\varphi}(k')\tilde{\varphi}(P'-k')\tilde{\varphi}^{\dagger}(k)\tilde{\varphi}^{\dagger}(P-k)\rangle \,, \tag{41}$$

where $k = (k_0, \mathbf{0})$ and $P - k = (E - k_0, \mathbf{0})$, with similar relations for the final state variables. We can express the momentum-space correlator as a series in Feynman diagrams as shown in Fig. 3. At leading order, the contribution comes from the product of two single particle propagators (see (a1) and (a2) of Fig. 3), which gives $C^{(0)}_{\mathrm{2pt,th}} = 1$.

The next-to-leading order (NLO) contribution involves a single insertion of $\mathcal{M}^{(1)}$ (see Fig. 3 (b)). Evaluating the k_0 and k_0' integrals, keeping only the terms which contribute to the threshold energy, we can write the next-to-leading

order contribution as

$$C^{(1)}_{\text{2pt,th}}(0) = -\frac{\xi}{L^3}\int\frac{\mathrm{d}E}{2\pi}\,\frac{i\mathcal{M}^{(1)}(E)}{E^2(E-2m+i\epsilon)^2} = -\frac{\xi}{L^3}\frac{\partial}{\partial E}\left(\frac{1}{E^2}\,\mathcal{M}^{(1)}(E)\right)\Big|_{E=2m}, \tag{42}$$

where we evaluated the integral by closing the contour in the lower-half E-plane. The next-to-next-to-leading order (N2LO) contribution amounts to replacing $\mathcal{M}^{(1)}$ as follows

$$\begin{aligned} i\mathcal{M}^{(1)}(E) &\longrightarrow i\mathcal{M}^{(1)}(E)\frac{1}{L^3}\xi\sum_{\mathbf{k}}\int\frac{\mathrm{d}k_0}{2\pi}\,\frac{i}{k^2-m^2+i\epsilon}\,\frac{i}{(P-k)^2-m^2+i\epsilon}\,i\mathcal{M}^{(1)}(E) \\ &\longrightarrow i\mathcal{M}^{(2)}(E) - i\left(\mathcal{M}^{(1)}(E)\right)^2 F(E,L), \end{aligned} \tag{43}$$

where we replaced the loop sum by it's infinite-volume counterpart and introduced $F(E,L)$ as defined in Eq. (3).

$$C^{(2)}_{\text{2pt,th}}(0) = -\frac{\xi}{L^3}\int\frac{\mathrm{d}E}{2\pi}\,\frac{i}{E^2(E-2m+i\epsilon)^2}\left[\mathcal{M}^{(2)}(E) - \left(\mathcal{M}^{(1)}(E)\right)^2 F(E,L)\right] \tag{44}$$

The second term in Eq. (44) contains an additional pole in E at $2m$ due to the zero mode of $F(E,L)$. This forces us to introduce a new finite-volume function with this mode removed and where the integral is evaluated using the principal-valued prescriptions, denoted here by $\mathcal{P}$,

$$F'(E,L) = \xi\left[\frac{1}{L^3}\sum\!\!\!\!\!\!\int_{\mathbf{k}\neq\mathbf{0}}\right]\mathcal{P}\frac{1}{2\omega_{\mathbf{k}}\,E(E-2\omega_{\mathbf{k}})} \tag{45}$$

such that

$$F(E,L) = i\frac{\xi q}{8\pi E} + \frac{\xi}{2mL^3}\frac{1}{E(E-2m+i\epsilon)} + F'(E,L). \tag{46}$$

We removed the imaginary part of $F(E,L)$ since it is zero in the threshold limit. The middle term of Eq. (46) increases the multiplicity of the simple pole at $E=2m$, while the term proportional to $F'(E,L)$ remains as before in Eq. (42). Evaluating Eq. (44) yields the threshold behavior

$$\begin{aligned} C^{(2)}_{\text{2pt,th}}(0) = &-\frac{\xi}{L^3}\frac{\partial}{\partial E}\left\{\frac{1}{E^2}\left[\mathcal{M}^{(2)}(E) - \left(\mathcal{M}^{(1)}(E)\right)^2 F'(E,L)\right]\right\}\Big|_{E=2m} \\ &+\frac{\xi^2}{2mL^6}\frac{1}{2!}\frac{\partial^2}{\partial E^2}\left[\frac{1}{E^3}\left(\mathcal{M}^{(1)}(E)\right)^2\right]\Big|_{E=2m}. \end{aligned} \tag{47}$$

We can repeat this procedure for higher-order diagrams. For example, in Fig. 3 (d), we replace each finite-volume sum with an infinite-volume loop and F-function. We simply state the result,

$$\begin{aligned} C^{(3)}_{\text{2pt,th}}(0) = &-\frac{\xi}{L^3}\frac{\partial}{\partial E}\left\{\frac{1}{E^2}\left[\mathcal{M}^{(3)}(E) - 2\mathcal{M}^{(1)}(E)\mathcal{M}^{(2)}(E)F'(E,L) + \left(\mathcal{M}^{(1)}(E)\right)^3 F'^2(E,L)\right]\right\}\Big|_{E=2m} \\ &-\frac{\xi^2}{2mL^6}\frac{1}{2!}\frac{\partial^2}{\partial E^2}\left\{\frac{1}{E^3}\left[-2\mathcal{M}^{(1)}(E)\mathcal{M}^{(2)}(E) + \left(2\mathcal{M}^{(1)}(E)\right)^3 F'(E,L)\right]\right\}\Big|_{E=2m} \\ &-\frac{\xi^3}{(2m)^2L^9}\frac{1}{3!}\frac{\partial^3}{\partial E^3}\left\{\frac{1}{E^4}\left(\mathcal{M}^{(1)}(E)\right)^3\right\}_{E=2m}, \end{aligned} \tag{48}$$

and follow the pattern for all higher-order contributions.

We combine the results of Eqs. (40), (42),(47), and (48), including higher order diagrams which contribute to $\mathcal{O}(\mathcal{M}^3)$ so that we may sum $\mathcal{M} = \mathcal{M}^{(1)} + \mathcal{M}^{(2)} + \mathcal{M}^{(3)} + \cdots$, we arrive at

$$\begin{aligned} C_{\text{2pt,th}}(0) = 1 &-\frac{\xi}{L^3}\frac{\partial}{\partial E}\left\{\frac{1}{E^2}\Big[\mathcal{M}(E) - \mathcal{M}^2(E)F'(E,L) + \mathcal{M}^3(E)F'^2(E,L)\Big]\right\}_{E=2m} \\ &-\frac{\xi^2}{2mL^6}\frac{1}{2!}\frac{\partial^2}{\partial E^2}\left\{\frac{1}{E^3}\Big[-\mathcal{M}^2(E) + 2\mathcal{M}^3(E)F'(E,L)\Big]\right\}_{E=2m} \\ &-\frac{\xi^3}{(2m)^2L^9}\frac{1}{3!}\frac{\partial^3}{\partial E^3}\left\{\frac{1}{E^4}\,\mathcal{M}^3(E)\right\}_{E=2m} + \mathcal{O}(\mathcal{M}^4) \end{aligned} \tag{49}$$

In the following, we want to express the expansion as a series in $1/L$ up through $\mathcal{O}(L^{-3})$, so we neglect terms of higher power. However, $F'(E,L)$ contains volume-dependence, which can be obtained from Eq. (6) by removing the zero mode contribution,

$$\begin{aligned} F'(2m,L) &= -\frac{\xi}{16\pi^2 mL}\mathcal{I}, \\ \frac{\partial}{\partial E}F'(E,L)\Big|_{E=2m} &= -\frac{\xi L}{64\pi^4}\mathcal{J} + \frac{\xi}{32\pi^2 m^2 L}\mathcal{I}, \\ \frac{\partial^2}{\partial E^2}F'(E,L)\Big|_{E=2m} &= -\frac{\xi m L^3}{128\pi^6}\mathcal{K} + \frac{\xi L}{128\pi^4 m}\mathcal{J} - \frac{\xi}{32\pi^2 m^3 L}\mathcal{I}, \end{aligned} \tag{50}$$

where $\mathcal{I}$, $\mathcal{J}$, and $\mathcal{K}$ are the geometric constants introduced in Eq. (7), and all exponentially suppressed terms are neglected. Derivatives of $F'(E,L)$ yield volume enhancing effects, which causes terms in the expansion at different orders in the Bethe-Salpeter kernels to mix when expressed as an expansion in $1/L$. One can convince themselves that through $\mathcal{O}(L^{-3})$, only these terms given in Eq. (49) contribute. For example, the next order term contributing to the single derivative term of Eq. (49) is $\sim \partial_E\left(\mathcal{M}^4 F'^3\right)$, and volume enhancements arise in the form $\sim F'^2\partial_E F' \sim 1/L$ according to Eq. (50). Therefore, this term and all higher order terms in the first derivative term contribute to $\mathcal{O}(1/L^4)$. Similar analyses on the higher derivative terms confirm that they all contribute beginning at $\mathcal{O}(1/L^4)$.

Substituting Eq. (50), along with $\mathcal{M}(E) = 8\pi E a/\xi$ for the scattering amplitude, into Eq. (49), and rearranging as a series in $1/L$, we find for the wavefunction renormalization

$$Z_0 = C_{\text{2pt,th}}(0) = 1 - \left(\frac{a}{\pi L}\right)^2 \mathcal{J} - \frac{2\pi^4}{m^2 a^2}\left(\frac{a}{\pi L}\right)^3 - 2(\mathcal{K} - \mathcal{I}\mathcal{J})\left(\frac{a}{\pi L}\right)^3 + \mathcal{O}(L^{-4}). \tag{51}$$

The first sub-leading correction at $\mathcal{O}(L^{-3})$ is due to the leading-order amplitude Fig. 3 (b), whereas the correction at $\mathcal{O}(L^{-2})$ arises from volume enhancements in the one-loop diagram, Fig. 3 (c).

B. Three-point correlator

The three-point correlator at threshold involves the matrix element

$$\langle \tilde{\varphi}_{\mathbf{0}}^2(t)\mathcal{J}_1(0)\tilde{\varphi}_{\mathbf{0}}^{\dagger\,2}(-t)\rangle\,\big|_{\text{th}} = \int\frac{\mathrm{d}E'}{2\pi}\int\frac{\mathrm{d}E}{2\pi}\int\frac{\mathrm{d}k_0'}{2\pi}\int\frac{\mathrm{d}k_0}{2\pi}e^{-iE't'+iEt}\,\langle\tilde{\varphi}(P'-k')\tilde{\varphi}(k')\mathcal{J}_1(0)\tilde{\varphi}(P-k)\tilde{\varphi}(k)\rangle\,\big|_{\text{th}}, \tag{52}$$

where all the four-momenta have zero spatial component. The momentum-space correlator on the right-hand side of Eq. (52) is now expressed as a series of Feynman amplitudes ordered in the strong coupling, with the label 'th' indicating that we will throw away all non-threshold contributions.

The LO contribution arises from diagrams (a) of Fig. 4, with each diagram having a multiplicity $\times 2$ to account for how the current can couple to one of the particles,

$$\begin{aligned} C^{(0)}_{\text{3pt,th}}(0,0) &= \frac{(2m)^2\xi}{L^6}\left(2\times\frac{g}{2m\xi}L^3\right)\int\frac{\mathrm{d}E'}{2\pi}\int\frac{\mathrm{d}E}{2\pi}\,\frac{i}{E'(E'-2m+i\epsilon)}\,\frac{i}{E(E-2m+i\epsilon)} \\ &= \frac{g}{2m\xi L^3}. \end{aligned} \tag{53}$$

We find that the three-point function at this order is the two-point function at the same order, scaled by the volume and the coupling of the hadron to the external current. In addition to the previously mentioned factor of 2, we must include an additional factor of $1/\xi$ attributed to the fact that the particles are identical. The factor of L^3 comes from a momentum-conserving delta function.

At NLO, we must consider two diagrams of the type discussed at the beginning of this section, Fig. 4 (b1) and (b2), where the current couple to a single hadron in the final state. As mentioned above, these do not contribute to the all orders derivation but must certainly be included in a finite-order calculation. We find their contribution to the three-point correlator to be

$$C^{(1)}_{\text{3pt,th}}(0,0) = -2\times\frac{g}{2m\xi L^3}\frac{\xi}{L^3}\frac{\partial}{\partial E}\left(\frac{1}{E^2}\,\mathcal{M}^{(1)}(E)\right)\Big|_{E=2m}. \tag{54}$$

The factor of 2 arises because the diagrams (b1) and (b2) are equal when evaluated at $E = E' = 2m$. At this order, the correlator is the two-point correlator at the same order mulitplied by a factor to account for the current attached

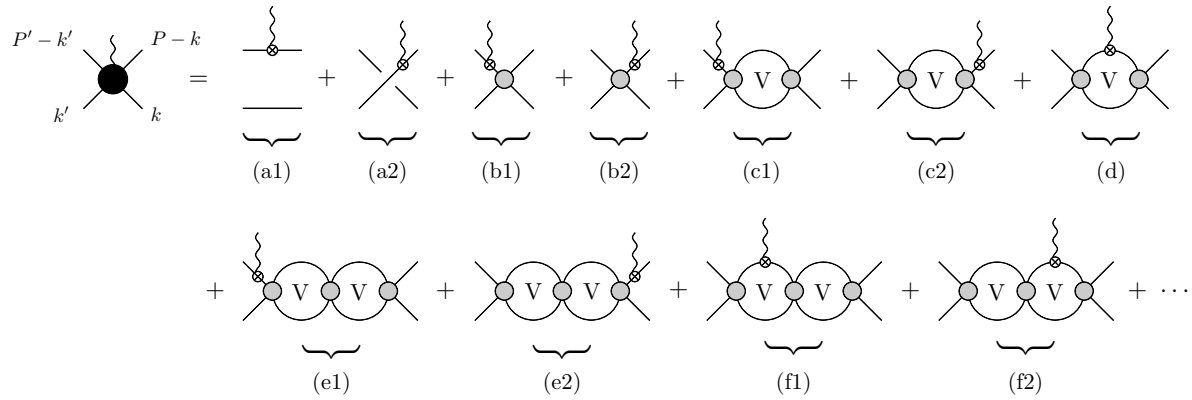

Figure 4. Expansion of momentum space finite-volume three-point correlator in terms of the Bethe-Salpeter kernels. Since the particles are identical, diagrams (a-c), and (e) contain a multiplicity $\times 2$ to account for the current probing both the upper and lower legs. Triangle diagrams in (d) and (f) do not contain a multiplicity as there is only a single contribution for identical particles.

to the external leg. This pattern continues for the N2LO diagrams (c1), (c2) of Fig. 4, and at N3LO in (e1), (e2). A new contribution arises at N2LO and N3LO, a triangle amplitude denoted in Fig. 4 (d) and (f1), (f2), respectively.

At N2LO, diagram (d) takes the general form

$$C_{\text{3pt,th}}^{(2,\text{d})}(0,0) = \frac{(2m)^2\xi}{L^6}\frac{g}{(2m)^2}\int\frac{\mathrm{d}E'}{2\pi}\int\frac{\mathrm{d}E}{2\pi}\frac{i}{E'(E'-2m+i\epsilon)}\frac{i}{E(E-2m+i\epsilon)} \times\left[\frac{1}{g}\mathcal{W}_{\text{df,1B}}^{(2)}(E',E)+\mathcal{M}^{(1)}(E')G(E',E,L)\mathcal{M}^{(1)}(E)\right], \tag{55}$$

where we evaluated the integrals over the momenta k, and replaced the finite-volume sum with a sum-integral identity, defining the N2LO 1-Body contribution to $\mathcal{W}_{\text{df}}$,

$$\mathcal{W}_{\text{df,1B}}^{(2)}(E',E) = g\,i\mathcal{M}^{(1)}(E')i\mathcal{M}^{(1)}(E)\int\frac{\mathrm{d}^4k}{(2\pi)^4}\frac{i}{k^2-m^2+i\epsilon}\frac{i}{E'(E'-2\omega_{\mathbf{k}}+i\epsilon)}\frac{i}{E(E-2\omega_{\mathbf{k}}+i\epsilon)}, \tag{56}$$

and the finite-volume G function

$$\begin{aligned} G(E',E,L) &= -\left[\frac{1}{L^3}\sum\!\!\!\!\!\!\int_{\mathbf{k}}\right]\frac{1}{2\omega_{\mathbf{k}}}\frac{i}{E'(E'-2\omega_{\mathbf{k}}+i\epsilon)}\frac{i}{E(E-2\omega_{\mathbf{k}}+i\epsilon)} \\ &\equiv \mathrm{Im}\,G(E',E,L)+\frac{1}{2mL^3}\frac{1}{E'(E'-2m+i\epsilon)}\frac{1}{E(E-2m+i\epsilon)}+G'(E',E,L). \end{aligned} \tag{57}$$

As for the F-function, we defined $G'(E',E,L)$ as the function without the zero-mode pole or imaginary part

$$G'(E',E,L) \equiv -\left[\frac{1}{L^3}\sum\!\!\!\!\!\!\int_{\mathbf{k}\neq\mathbf{0}}\right]\mathcal{P}\frac{1}{2\omega_{\mathbf{k}}}\frac{i}{E'(E'-2\omega_{\mathbf{k}}+i\epsilon)}\frac{i}{E(E-2\omega_{\mathbf{k}}+i\epsilon)}. \tag{58}$$

The imaginary part cancels identically with that in $\mathcal{W}_{\text{df,1B}}^{(2)}$, and the zero-mode pole increases the multiplicity of the poles at $E'=E=2m$. Evaluating the integrals as before, we arrive at the N2LO contribution

$$\begin{aligned} C_{\text{3pt,th}}^{(2)}(0,0) = {}& \frac{\xi g}{(2m)^2L^6}\left[\frac{1}{g}\mathrm{Re}\left(\mathcal{W}_{\text{df,1B}}^{(2)}(E,E)\right)+\left(\mathcal{M}^{(1)}(E)\right)^2G'(E,E,L)\right]_{E=2m}+\frac{g\xi}{2mL^9}\left[\frac{\partial}{\partial E}\left(\frac{1}{E^2}\mathcal{M}^{(1)}(E)\right)_{E=2m}\right]^2 \\ & -2\times\frac{g}{2mL^6}\frac{\partial}{\partial E}\left(\frac{1}{E^2}\left[\mathcal{M}^{(2)}(E)-\left(\mathcal{M}^{(1)}(E)\right)^2F(E,L)\right]\right)\Bigg|_{E=2m} \\ & +2\times\frac{g\xi}{(2m)^2L^9}\frac{1}{2!}\frac{\partial^2}{\partial E^2}\left(\frac{1}{E^3}\left(\mathcal{M}^{(1)}(E)\right)^2\right)_{E=2m}. \end{aligned} \tag{59}$$

Given our definition of the two-hadron form-factor, Eq. (13), the term proportional to $\mathcal{W}^{(2)}_{\text{df,1B}}$ contributes to the correlator involving a current coupling to a two-hadron state

$$\frac{\xi}{(2m)^2L^6}\text{Re}\,\mathcal{W}^{(2)}_{\text{df}}(2m,2m)=\frac{(8\pi a)^2}{\xi L^6}\mathcal{F}_0. \tag{60}$$

The diagrams (f) of Fig. 4 follow the manipulations, with the addition of the scalar bubble loop giving the finit-volume F functions. We will forgo writing these diagrams, and just use them when summing all terms in the correlator.

As in Sec. III A, we will partially sum to all-orders by including higher diagrams so that we may use Eq. (39). Performing this sum, we arrive at

$$\begin{aligned}\frac{2m\xi L^3}{g}C_{\text{3pt,th}}(0,0)=1&-2\times\frac{\xi}{L^3}\frac{\partial}{\partial E}\left\{\frac{1}{E^2}\Big[\mathcal{M}(E)-\mathcal{M}^2(E)F'(E,L)+\mathcal{M}^3(E)F'^{\,2}(E,L)\Big]\right\}_{E=2m}\\
&-2\times\frac{\xi^2}{2mL^6}\frac{1}{2!}\frac{\partial^2}{\partial E^2}\left\{\frac{1}{E^3}\Big[-\mathcal{M}^2(E)+2\mathcal{M}^3(E)F'(E,L)\Big]\right\}_{E=2m}\\
&-2\times\frac{\xi^3}{(2m)^2L^9}\frac{1}{3!}\frac{\partial^3}{\partial E^3}\left\{\frac{1}{E^4}\,\mathcal{M}^3(E)\right\}_{E=2m}\\
&+\frac{1}{2m\xi L^3}\left[\frac{1}{g}\mathcal{W}_{\text{df,1B}}(E,E)+\mathcal{M}^2(E)G'(E,E,L)-2\mathcal{M}^3(E)G'(E,E,L)F'(E,L)\right]_{E=2m}\\
&-\frac{1}{2mL^6}\mathcal{M}(2m)\frac{\partial}{\partial E}\left[\frac{1}{E^2}\Big(\mathcal{M}^2(E)G'(2m,E,L)\Big)\right]_{E=2m}\\
&-\frac{1}{L^6}\left[\frac{\partial}{\partial E}\left(\frac{1}{E^2}\mathcal{M}(E)\right)_{E=2m}\right]^2-2\times\frac{1}{L^6}\frac{\partial}{\partial E}\left(\frac{1}{E^2}\mathcal{M}(E)\right)\frac{\partial}{\partial E}\left(\frac{1}{E^2}\mathcal{M}^2(E)F'(E,L)\right)_{E=2m}\\
&-\frac{1}{2mL^9}\frac{1}{2!}\frac{\partial}{\partial E}\left(\frac{1}{E^2}\mathcal{M}(E)\right)_{E=2m}\frac{\partial^2}{\partial E^2}\left(\frac{1}{E^3}\mathcal{M}^2(E)\right)_{E=2m}+\mathcal{O}(\mathcal{M}^4).\end{aligned} \tag{61}$$

Finite-volume functions enhance the volume dependence, with F' at threshold given in Eq. (50) and for G' ,

$$G'(2m,2m,L)=\frac{L}{128\pi^4 m}\mathcal{J},\quad \frac{\partial}{\partial E}G(2m,E,L)\Big|_{E=2m}=\frac{L^3}{512\pi^6}\mathcal{K}-\frac{L}{512\pi^4m^2}\mathcal{J}, \tag{62}$$

Keeping only terms contributing to $\mathcal{O}(L^{-3})$, and evaluating all quantities at threshold, the three-point correlator reduces to the series

$$\frac{2m\xi L^3}{g}C_{\text{3pt,th}}(0,0)=1-\left(\frac{a}{\pi L}\right)^2\mathcal{J}-\frac{1}{\xi}\frac{2\pi^4}{m^2a^2}\left(\frac{a}{\pi L}\right)^3-2(\mathcal{K}-\mathcal{I}\mathcal{J})\left(\frac{a}{\pi L}\right)^3+\mathcal{O}(L^{-4}). \tag{63}$$

Combining the results Eqs. (51) and (63), we arrive at the threshold expansion of the matrix element

$$\begin{aligned}L^3\langle E_0,L|\,\mathcal{J}(0)\,|E_0,L\rangle&=\frac{L^3}{Z_0}C_{\text{3pt,th}}(0,0)\\
&=\frac{g}{2m\xi}\frac{1-\left(\frac{a}{\pi L}\right)^2\mathcal{J}-\frac{1}{\xi}\frac{2\pi^4}{m^2a^2}\left(\frac{a}{\pi L}\right)^3-2(\mathcal{K}-\mathcal{I}\mathcal{J})\left(\frac{a}{\pi L}\right)^3+\mathcal{O}(L^{-4})}{1-\left(\frac{a}{\pi L}\right)^2\mathcal{J}-\frac{2\pi^4}{m^2a^2}\left(\frac{a}{\pi L}\right)^3-2(\mathcal{K}-\mathcal{I}\mathcal{J})\left(\frac{a}{\pi L}\right)^3+\mathcal{O}(L^{-4})}\\
&=\frac{g}{2m\xi}\left[1-\frac{2\pi^4}{m^2a^2}\left(\frac{a}{\pi L}\right)^3+\mathcal{O}(L^{-4})\right],\end{aligned} \tag{64}$$

where we recall that $\xi=1/2$. Equation (64) is identical to what was found for the threshold expansion Eq. (26). Fig. 5 shows the leading order in $1/L$ contributions from each diagram to the matrix element. We conclude that the discrepancy with Ref. [87] arises from two sources: (i) diagrams where the external legs are probed contribute to the same order as the one-body insertion in the intermediate states of the triangle diagrams, with a factor of $\times 2$ which switches the sign on these terms. (ii) the wavefunction renormalization contains identical terms, which cancel order-by-order in the expansion. In addition to the cancellations, diagrams where the current connects to the external legs provide additional terms which enhance the finite-volume dependence beginning at $\mathcal{O}(L^{-3})$. It is straightforward to see that if we neglect the diagrams where the current probes the external legs, (b), (c), and (e) of Fig. 4, and neglect the wavefunction renormalization, we recover the $1/L$ expansion of the matrix element as shown in Ref. [87].

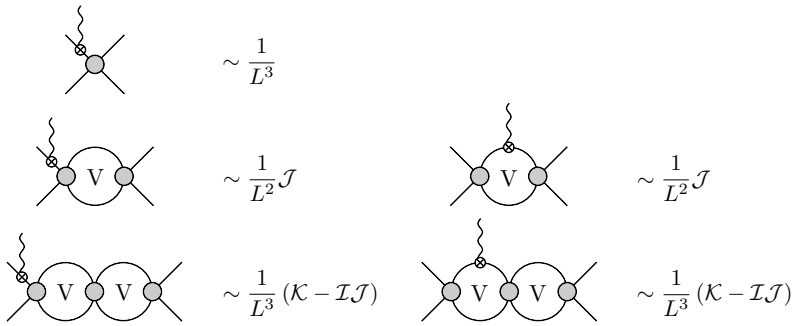

Figure 5. Leading finite-volume scaling for contributing diagrams to the matrix element from the three-point correlator. Diagrams on the left have identical scaling to those of the corresponding two-point correlator of the same topology. Loop effects induce finite-volume enhancements.

IV. SUMMARY

Understanding the structure of strongly interacting resonances and bound states requires knowledge of two-hadron electroweak transition amplitudes. A framework presented in Ref. [76, 77] relates finite volume matrix elements, which can be computed via lattice QCD, to infinite volume $\mathbf{2}+\mathcal{J}\to\mathbf{2}$ amplitudes. The formalism is non-perturbative in the strong interactions while considering a single external current insertion, and it provides a mapping between matrix element and infinite-volume $\mathbf{2}+\mathcal{J}\to\mathbf{2}$ amplitudes. To gain confidence of the formalism, consistency checks were performed in Ref. [79] which studied matrix elements of bound states and verified that the expected limit was recovered. Furthermore, it was proved that the electromagnetic charge is protected from finite-volume effects. Following the work in Ref. [79], we continued our study to the non-relativistic limit of the matrix element, above the two-hadron threshold. We found that the matrix element near threshold can be expressed as a series in $1/L$ for a fixed scattering length. We numerically verified that the all-orders expression asymptotically approaches the expansion coefficients derived for large L.

We compared our result with that of Ref. [87], and found a significant discrepancy beginning at the first non-trivial correction. In order to ascertain the expansion derived, we performed an alternative derivation using time-ordered perturbation theory. It was found that if one neglected diagrams where the current probes an external leg, as well as neglected corrections from the wavefunction renormalization, that the expansion derived in Ref. [87] was recovered. However, for a systematically controlled expansion, one must include these contributions. When taking into account diagrams probing external legs and corrections induced by the wavefunction renormalization, the expansion derived in Sec. II B was recovered.

V. ACKNOWLEDGEMENTS

We thank Will Detmold for useful discussions. R.A.B. is supported in part by USDOE grant No. DE-AC05-06OR23177, under which Jefferson Science Associates, LLC, manages and operates Jefferson Lab. R.A.B. also acknowledges support from the USDOE Early Career award, contract de-sc0019229.

Appendix A: Imaginary part of triangle diagram

In this appendix, we show that the imaginary part of the triangle diagram at zero-momentum transfer gives the result shown in Eq. (17). We will freely absorb all regular terms into a single smooth function since only the singular contributions will yield the imaginary part. Generally, the triangle amplitude is a Feynman diagram

$$G_\infty(P',P)=i\int\frac{\mathrm{d}^4k}{(2\pi)^4}\,\frac{1}{k^2-m^2+i\epsilon}\,\frac{1}{(P'-k)^2-m^2+i\epsilon}\,\frac{1}{(P-k)^2-m^2+i\epsilon}, \tag{A1}$$

where $P=(E,\mathbf{P})$ and $P'=(E',\mathbf{P}')$ are the initial and final four-momenta, respectively. Two of the vertices correspond to Bethe-Salpeter kernels, while the third is the $\mathbf{1}+\mathcal{J}\to\mathbf{1}$ amplitude. After on-shell projection, these are removed from the integral, and the kernels are summed to give the $\mathbf{2}\to\mathbf{2}$ scattering amplitude, while the on-shell

$\mathbf{1} + \mathcal{J} \to \mathbf{1}$ amplitude gives the form-factor $f(Q^2)$. We first perform the k^0-integral by closing the contour in the lower-half k^0-plane, finding

$$G_\infty(P', P) = \int \frac{\mathrm{d}^3\mathbf{k}}{(2\pi)^3} \frac{1}{2\omega_\mathbf{k}} \frac{1}{(P'-k)^2 - m^2 + i\epsilon} \frac{1}{(P-k)^2 - m^2 + i\epsilon} + \int \frac{\mathrm{d}^3\mathbf{k}}{(2\pi)^3} \mathcal{S}(\mathbf{k}, P', P), \tag{A2}$$

where $\mathcal{S}(\mathbf{k}, P', P)$ is a regular function in $\mathbf{k}$ in the elastic kinematic domain of P and P', therefore it will not contribute to the imaginary part of the triangle amplitude. We now consider the situation of zero momentum transfer, and boost the system to its center-of-momentum frame, such that $P = P' = E$. The triangle amplitude reduces to

$$G_\infty(E, E) = \int \frac{\mathrm{d}^3\mathbf{k}}{(2\pi)^3} \frac{1}{2\omega_\mathbf{k}} \frac{1}{E^2(E - 2\omega_\mathbf{k} + i\epsilon)^2} + \int \frac{\mathrm{d}^3\mathbf{k}}{(2\pi)^3} \mathcal{S}(\mathbf{k}, E, E). \tag{A3}$$

It is convenient to rewrite the integrand of Eq. (A3) in terms of k^2, which w manipulate as

$$\frac{1}{2\omega_\mathbf{k}} \frac{1}{E^2(E - 2\omega_\mathbf{k} + i\epsilon)^2} = \frac{1}{2\omega_\mathbf{k}} \frac{(E + 2\omega_\mathbf{k})^2}{(4E)^2(q^2 - k^2 + i\epsilon)^2} = \frac{1}{4E} \frac{1}{(q^2 - k^2 + i\epsilon)^2} + \mathcal{O}\left(\left(k^2 - q^2\right)^0\right), \tag{A4}$$

where we concentrate on the leading pole term, and absorb all terms regular in k^2 with the function $\mathcal{S}(\mathbf{k}, E, E)$, which we will call $\mathcal{S}'(\mathbf{k}, E, E)$. We are left with

$$G_\infty(E, E) = \frac{1}{8\pi^2 E} \int_0^\infty \mathrm{d}k \frac{k^2}{(q^2 - k^2 + i\epsilon)^2} + \int \frac{\mathrm{d}^3\mathbf{k}}{(2\pi)^3} \mathcal{S}'(\mathbf{k}, E, E). \tag{A5}$$

The first term of Eq. (A5) yields an imaginary part, which we extract by writing the integral as a contour integral,

$$\int_0^\infty \mathrm{d}k \frac{k^2}{(q^2 - k^2 + i\epsilon)^2} = \frac{1}{2} \int_{-\infty}^\infty \mathrm{d}k \frac{k^2}{(q^2 - k^2 + i\epsilon)^2} = \frac{1}{2} \oint \mathrm{d}k \frac{k^2}{(k - q - i\epsilon)^2 (k + q + i\epsilon)^2}, \tag{A6}$$

where the contour is taken in the upper-half k-plane, and the radial part is zero as $|k| \to \infty$. Evaluating the integral, we pick up the residue at the pole $k = q - i\epsilon$,

$$\oint \mathrm{d}k \frac{k^2}{(k - q - i\epsilon)^2 (k + q + i\epsilon)^2} = 2\pi i \frac{\mathrm{d}}{\mathrm{d}k} \frac{k^2}{(k+q)^2}\bigg|_{k=q} = i\frac{\pi}{2q}. \tag{A7}$$

Since the second term of Eq. (A5) is a real function, the imaginary part of G_∞ is

$$\mathrm{Im}\, G_\infty(E, E) = \frac{1}{32\pi E q}, \tag{A8}$$

which is our desired result.

[1] S. Durr *et al.*, Science **322**, 1224 (2008), arXiv:0906.3599 [hep-lat].
[2] Z. Fodor and C. Hoelbling, Rev. Mod. Phys. **84**, 449 (2012), arXiv:1203.4789 [hep-lat].
[3] S. Borsanyi *et al.*, Science **347**, 1452 (2015), arXiv:1406.4088 [hep-lat].
[4] M. Luscher, Commun. Math. Phys. **105**, 153 (1986).
[5] M. Luscher, Nucl. Phys. **B354**, 531 (1991).
[6] K. Rummukainen and S. A. Gottlieb, Nucl. Phys. **B450**, 397 (1995), arXiv:hep-lat/9503028 [hep-lat].
[7] C. h. Kim, C. T. Sachrajda, and S. R. Sharpe, Nucl. Phys. **B727**, 218 (2005), arXiv:hep-lat/0507006 [hep-lat].
[8] S. He, X. Feng, and C. Liu, JHEP **07**, 011 (2005), arXiv:hep-lat/0504019 [hep-lat].
[9] L. Leskovec and S. Prelovsek, Phys. Rev. **D85**, 114507 (2012), arXiv:1202.2145 [hep-lat].
[10] M. T. Hansen and S. R. Sharpe, Phys. Rev. **D86**, 016007 (2012), arXiv:1204.0826 [hep-lat].
[11] R. A. Briceño and Z. Davoudi, Phys. Rev. **D88**, 094507 (2013), arXiv:1204.1110 [hep-lat].
[12] R. A. Briceño, Z. Davoudi, and T. C. Luu, Phys. Rev. **D88**, 034502 (2013), arXiv:1305.4903 [hep-lat].
[13] R. A. Briceño, Phys. Rev. **D89**, 074507 (2014), arXiv:1401.3312 [hep-lat].
[14] F. Romero-Lopez, A. Rusetsky, and C. Urbach, Phys. Rev. **D98**, 014503 (2018), arXiv:1802.03458 [hep-lat].
[15] J. J. Dudek, R. G. Edwards, M. J. Peardon, D. G. Richards, and C. E. Thomas, Phys. Rev. **D83**, 071504 (2011), arXiv:1011.6352 [hep-ph].

[16] S. R. Beane, E. Chang, W. Detmold, H. W. Lin, T. C. Luu, K. Orginos, A. Parreno, M. J. Savage, A. Torok, and A. Walker-Loud (NPLQCD), Phys. Rev. **D85**, 034505 (2012), arXiv:1107.5023 [hep-lat].
[17] C. Pelissier and A. Alexandru, Phys. Rev. **D87**, 014503 (2013), arXiv:1211.0092 [hep-lat].
[18] J. J. Dudek, R. G. Edwards, and C. E. Thomas (Hadron Spectrum), Phys. Rev. **D87**, 034505 (2013), [Erratum: Phys. Rev.D90,no.9,099902(2014)], arXiv:1212.0830 [hep-ph].
[19] L. Liu, K. Orginos, F.-K. Guo, C. Hanhart, and U.-G. Meissner, Phys. Rev. **D87**, 014508 (2013), arXiv:1208.4535 [hep-lat].
[20] S. R. Beane *et al.* (NPLQCD), Phys. Rev. **C88**, 024003 (2013), arXiv:1301.5790 [hep-lat].
[21] K. Orginos, A. Parreno, M. J. Savage, S. R. Beane, E. Chang, and W. Detmold, Phys. Rev. **D92**, 114512 (2015), arXiv:1508.07583 [hep-lat].
[22] E. Berkowitz, T. Kurth, A. Nicholson, B. Joo, E. Rinaldi, M. Strother, P. M. Vranas, and A. Walker-Loud, Phys. Lett. **B765**, 285 (2017), arXiv:1508.00886 [hep-lat].
[23] C. B. Lang, D. Mohler, S. Prelovsek, and R. M. Woloshyn, Phys. Lett. **B750**, 17 (2015), arXiv:1501.01646 [hep-lat].
[24] J. Bulava, B. Fahy, B. Horz, K. J. Juge, C. Morningstar, and C. H. Wong, Nucl. Phys. **B910**, 842 (2016), arXiv:1604.05593 [hep-lat].
[25] B. Hu, R. Molina, M. Doring, and A. Alexandru, Phys. Rev. Lett. **117**, 122001 (2016), arXiv:1605.04823 [hep-lat].
[26] C. Alexandrou, L. Leskovec, S. Meinel, J. Negele, S. Paul, M. Petschlies, A. Pochinsky, G. Rendon, and S. Syritsyn, Phys. Rev. **D96**, 034525 (2017), arXiv:1704.05439 [hep-lat].
[27] G. S. Bali, S. Collins, A. Cox, and A. Schäfer, Phys. Rev. **D96**, 074501 (2017), arXiv:1706.01247 [hep-lat].
[28] M. L. Wagman, F. Winter, E. Chang, Z. Davoudi, W. Detmold, K. Orginos, M. J. Savage, and P. E. Shanahan, Phys. Rev. **D96**, 114510 (2017), arXiv:1706.06550 [hep-lat].
[29] C. W. Andersen, J. Bulava, B. Horz, and C. Morningstar, Phys. Rev. **D97**, 014506 (2018), arXiv:1710.01557 [hep-lat].
[30] R. Brett, J. Bulava, J. Fallica, A. Hanlon, B. Horz, and C. Morningstar, Nucl. Phys. **B932**, 29 (2018), arXiv:1802.03100 [hep-lat].
[31] M. Werner *et al.*, (2019), arXiv:1907.01237 [hep-lat].
[32] M. Mai, C. Culver, A. Alexandru, M. Doring, and F. X. Lee, (2019), arXiv:1908.01847 [hep-lat].
[33] D. J. Wilson, R. A. Briceno, J. J. Dudek, R. G. Edwards, and C. E. Thomas, Phys. Rev. Lett. **123**, 042002 (2019), arXiv:1904.03188 [hep-lat].
[34] D. J. Wilson, J. J. Dudek, R. G. Edwards, and C. E. Thomas, Phys. Rev. **D91**, 054008 (2015), arXiv:1411.2004 [hep-ph].
[35] J. J. Dudek, R. G. Edwards, C. E. Thomas, and D. J. Wilson (Hadron Spectrum), Phys. Rev. Lett. **113**, 182001 (2014), arXiv:1406.4158 [hep-ph].
[36] D. J. Wilson, R. A. Briceño, J. J. Dudek, R. G. Edwards, and C. E. Thomas, Phys. Rev. **D92**, 094502 (2015), arXiv:1507.02599 [hep-ph].
[37] J. J. Dudek, R. G. Edwards, and D. J. Wilson (Hadron Spectrum), Phys. Rev. **D93**, 094506 (2016), arXiv:1602.05122 [hep-ph].
[38] R. A. Briceño, J. J. Dudek, R. G. Edwards, and D. J. Wilson, Phys. Rev. Lett. **118**, 022002 (2017), arXiv:1607.05900 [hep-ph].
[39] G. Moir, M. Peardon, S. M. Ryan, C. E. Thomas, and D. J. Wilson, JHEP **10**, 011 (2016), arXiv:1607.07093 [hep-lat].
[40] R. A. Briceno, J. J. Dudek, R. G. Edwards, and D. J. Wilson, Phys. Rev. **D97**, 054513 (2018), arXiv:1708.06667 [hep-lat].
[41] A. Woss, C. E. Thomas, J. J. Dudek, R. G. Edwards, and D. J. Wilson, JHEP **07**, 043 (2018), arXiv:1802.05580 [hep-lat].
[42] A. J. Woss, C. E. Thomas, J. J. Dudek, R. G. Edwards, and D. J. Wilson, Phys. Rev. **D100**, 054506 (2019), arXiv:1904.04136 [hep-lat].
[43] M. T. Hansen and S. R. Sharpe, Phys. Rev. **D90**, 116003 (2014), arXiv:1408.5933 [hep-lat].
[44] M. T. Hansen and S. R. Sharpe, Phys. Rev. **D92**, 114509 (2015), arXiv:1504.04248 [hep-lat].
[45] M. Mai and M. Doring, Eur. Phys. J. **A53**, 240 (2017), arXiv:1709.08222 [hep-lat].
[46] H. W. Hammer, J. Y. Pang, and A. Rusetsky, JHEP **10**, 115 (2017), arXiv:1707.02176 [hep-lat].
[47] R. A. Briceno, M. T. Hansen, and S. R. Sharpe, Phys. Rev. **D95**, 074510 (2017), arXiv:1701.07465 [hep-lat].
[48] R. A. Briceno, M. T. Hansen, and S. R. Sharpe, Phys. Rev. **D99**, 014516 (2019), arXiv:1810.01429 [hep-lat].
[49] M. Mai and M. Doring, Phys. Rev. Lett. **122**, 062503 (2019), arXiv:1807.04746 [hep-lat].
[50] R. A. Briceño, M. T. Hansen, and S. R. Sharpe, Phys. Rev. **D98**, 014506 (2018), arXiv:1803.04169 [hep-lat].
[51] D. Guo, A. Alexandru, R. Molina, M. Mai, and M. Döring, Phys. Rev. **D98**, 014507 (2018), arXiv:1803.02897 [hep-lat].
[52] T. D. Blanton, F. Romero-López, and S. R. Sharpe, JHEP **03**, 106 (2019), arXiv:1901.07095 [hep-lat].
[53] B. Hörz and A. Hanlon, (2019), arXiv:1905.04277 [hep-lat].
[54] T. D. Blanton, F. Romero-López, and S. R. Sharpe, (2019), arXiv:1909.02973 [hep-lat].
[55] M. Mai, M. Döring, C. Culver, and A. Alexandru, (2019), arXiv:1909.05749 [hep-lat].
[56] C. Culver, M. Mai, R. Brett, A. Alexandru, and M. Döring, (2019), arXiv:1911.09047 [hep-lat].
[57] R. A. Briceno, J. J. Dudek, and R. D. Young, Rev. Mod. Phys. **90**, 025001 (2018), arXiv:1706.06223 [hep-lat].
[58] M. T. Hansen and S. R. Sharpe, Annual Review of Nuclear and Particle Science **69**, null (2019), arXiv:1901.00483 [hep-lat].
[59] L. Lellouch and M. Luscher, Commun. Math. Phys. **219**, 31 (2001), arXiv:hep-lat/0003023 [hep-lat].
[60] N. H. Christ, C. Kim, and T. Yamazaki, Phys. Rev. **D72**, 114506 (2005), arXiv:hep-lat/0507009 [hep-lat].
[61] R. A. Briceño, M. T. Hansen, and A. Walker-Loud, Phys. Rev. **D91**, 034501 (2015), arXiv:1406.5965 [hep-lat].
[62] R. A. Briceño and M. T. Hansen, Phys. Rev. **D92**, 074509 (2015), arXiv:1502.04314 [hep-lat].
[63] A. Agadjanov, V. Bernard, U.-G. Meißner, and A. Rusetsky, Nucl. Phys. **B910**, 387 (2016), arXiv:1605.03386 [hep-lat].
[64] T. Blum *et al.*, Phys. Rev. Lett. **108**, 141601 (2012), arXiv:1111.1699 [hep-lat].
[65] P. A. Boyle *et al.* (RBC, UKQCD), Phys. Rev. Lett. **110**, 152001 (2013), arXiv:1212.1474 [hep-lat].

[66] T. Blum *et al.*, Phys. Rev. **D91**, 074502 (2015), arXiv:1502.00263 [hep-lat].
[67] Z. Bai *et al.* (RBC, UKQCD), Phys. Rev. Lett. **115**, 212001 (2015), arXiv:1505.07863 [hep-lat].
[68] X. Feng, S. Aoki, S. Hashimoto, and T. Kaneko, Phys. Rev. **D91**, 054504 (2015), arXiv:1412.6319 [hep-lat].
[69] C. Andersen, J. Bulava, B. Hörz, and C. Morningstar, Nucl. Phys. **B939**, 145 (2019), arXiv:1808.05007 [hep-lat].
[70] R. A. Briceño, J. J. Dudek, R. G. Edwards, C. J. Shultz, C. E. Thomas, and D. J. Wilson, Phys. Rev. Lett. **115**, 242001 (2015), arXiv:1507.06622 [hep-ph].
[71] R. A. Briceño, J. J. Dudek, R. G. Edwards, C. J. Shultz, C. E. Thomas, and D. J. Wilson, Phys. Rev. **D93**, 114508 (2016), arXiv:1604.03530 [hep-ph].
[72] C. Alexandrou, L. Leskovec, S. Meinel, J. Negele, S. Paul, M. Petschlies, A. Pochinsky, G. Rendon, and S. Syritsyn, Phys. Rev. **D98**, 074502 (2018), arXiv:1807.08357 [hep-lat].
[73] N. H. Christ, X. Feng, G. Martinelli, and C. T. Sachrajda, Phys. Rev. **D91**, 114510 (2015), arXiv:1504.01170 [hep-lat].
[74] X. Feng, L.-C. Jin, X.-Y. Tuo, and S.-C. Xia, Phys. Rev. Lett. **122**, 022001 (2019), arXiv:1809.10511 [hep-lat].
[75] R. A. Briceño, Z. Davoudi, M. T. Hansen, M. R. Schindler, and A. Baroni, (2019), arXiv:1911.04036 [hep-lat].
[76] R. A. Briceño and M. T. Hansen, Phys. Rev. **D94**, 013008 (2016), arXiv:1509.08507 [hep-lat].
[77] A. Baroni, R. A. Briceño, M. T. Hansen, and F. G. Ortega-Gama, Phys. Rev. **D100**, 034511 (2019), arXiv:1812.10504 [hep-lat].
[78] V. Bernard, D. Hoja, U. G. Meissner, and A. Rusetsky, JHEP **09**, 023 (2012), arXiv:1205.4642 [hep-lat].
[79] R. A. Briceño, M. T. Hansen, and A. W. Jackura, (2019), arXiv:1909.10357 [hep-lat].
[80] S. R. Beane, P. F. Bedaque, A. Parreno, and M. J. Savage, Phys. Lett. **B585**, 106 (2004), arXiv:hep-lat/0312004 [hep-lat].
[81] Z. Davoudi and M. J. Savage, Phys. Rev. **D84**, 114502 (2011), arXiv:1108.5371 [hep-lat].
[82] R. A. Briceño, Z. Davoudi, T. Luu, and M. J. Savage, Phys. Rev. **D88**, 114507 (2013), arXiv:1309.3556 [hep-lat].
[83] S. R. Beane, W. Detmold, and M. J. Savage, Phys. Rev. **D76**, 074507 (2007), arXiv:0707.1670 [hep-lat].
[84] W. Detmold and M. J. Savage, Phys. Rev. **D77**, 057502 (2008), arXiv:0801.0763 [hep-lat].
[85] M. T. Hansen and S. R. Sharpe, Phys. Rev. **D93**, 014506 (2016), arXiv:1509.07929 [hep-lat].
[86] M. T. Hansen and S. R. Sharpe, Phys. Rev. **D93**, 096006 (2016), arXiv:1602.00324 [hep-lat].
[87] W. Detmold and M. Flynn, Phys. Rev. **D91**, 074509 (2015), arXiv:1412.3895 [hep-lat].